Biointerface Research in Applied Chemistry
Open-Access Journal (ISSN: 2069-5837)

Article
Volume 15, Issue 5, 2025, 64
https://doi.org/10.33263/BRIAC155.064

Achieving Pliable GaP/GaInP/GaAs/GaInAs Hybrid Semiconductors through Atom Doping: An Architectural Modeling via Quantum Chemical Study

Fatemeh Mollaamin [1,*]

[1] Department of Biomedical Engineering, Faculty of Engineering and Architecture, Kastamonu University, Kastamonu, Turkey
* Correspondence: fmollaamin@kastamonu.edu.tr;

Received: 13.04.2025; Accepted: 21.07.2025; Published: 9.08.2025

Abstract: This work aims to investigate heteroclusters of (Si, Zn, Ag)-Doped GaInP/GaInAs, which can attract considerable attention for storage energy in solar cells. A comprehensive investigation on energy grabbing by GaInP, SiGaInP, ZnGaInP, AgGaInP, GaInAs, SiGaInAs, ZnGaInAs, AgGaInAs was carried out including using DFT computations at the CAM–B3LYP–D3/6-311+G (d,p) level of theory. The atoms of P/As10, P/As14 extracted from ternary heteroclusters of GaInP and GaInAs have exhibited the fluctuation in the range of -1.5 to +1 coulomb with an average electric potential of about -20 a.u. Electromagnetic and thermodynamic properties of GaInP, SiGaInP, ZnGaInP, AgGaInP, GaInAs, SiGaInAs, ZnGaInAs, and AgGaInAs heteroclusters have been evaluated. In GaInP and GaInAs, the photo-excited electrons and holes are strongly bound by the excitons because of their large exciton binding energy as EoAgGaInX> EoZnGaInX> EoSiGaInX (X=P or As) due to their efficient exciton dissociation. Therefore, it can be considered that zinc and silver atoms in the functionalized ZnGaInP/As and AgGaInP/As might have more impressive sensitivity for accepting electrons in the process of the energy adsorption mechanism. The changes of Gibbs free energy versus dipole moment could detect the maximum efficiency of AgGaInP and AgGaInAs heteroclusters for energy storage in the solar cells through 〖ΔG〗_(f, AgGaInP)^o= –134.9792×103 kcal/mol and 〖ΔG〗_(f, AgGaInAs)^o= –132.1931×103 kcal/mol, respectively. It can be observed that doped heteroclusters of AgGaInX and ZnGaInX (X=P or As) might ameliorate the capability of GaInX(X=P or As) in solar cells for energy storage.

Keywords: heterocluster; solar cells, energy saving; materials modeling.

1. Introduction

The nitrides of group III in the periodic table have low sensitivity to ionizing radiation, which makes them appropriate materials for solar cell arrays for satellites. Therefore, space applications could also benefit as devices have shown stability in high radiation environments [1–4]. In addition, GaN offers promising characteristics for THz devices. Due to high power density and voltage breakdown limits, GaN is also emerging as a promising candidate for 5G cellular base station applications [5–8].

GaN with a high crystalline quality can be obtained by depositing a buffer layer at low temperatures [9,10]. Such high-quality GaN led to the discovery of p-type GaN [11], p–n

junction blue/UV-LEDs [5], and room-temperature stimulated emission [12]. This has led to the commercialization of high-performance blue LEDs and long-lifetime violet laser diodes, and to the development of nitride-based devices such as UV detectors and high-speed field-effect transistors [13]. GaN-based metal–oxide–semiconductor field-effect transistor (MOSFET) and metal–semiconductor field-effect transistor (MESFET) transistors also offer advantages, including lower loss in high power electronics, especially in automotive and electric car applications [14]. The U.S. Army Research Laboratory (ARL) provided the first measurement of the high-field electron velocity in GaN in 1999 [15]. Scientists at ARL experimentally obtained a peak steady-state velocity of 1.9×10^7 cm/s, with a transit time of 2.5 picoseconds, attained at an electric field of 225 kV/cm. With this information, the electron mobility was calculated, thus providing data for the design of GaN devices [16–24].

The ability to perform bandgap engineering with InGaN over a range that provides a good spectral match to sunlight makes InGaN suitable for solar photovoltaic cells. It is possible to grow multiple layers with different band gaps, as the material is relatively insensitive to defects introduced by a lattice mismatch between the layers. Metal-doping allows controlled atomic layer-by-layer growth of thin films with almost ideal characteristics, enabled by strain relaxation at the first atomic layer. The crystal's lattice structures match up, resembling a perfect crystal, with corresponding luminosity [25–31]. Ultrafast exciton and charge-carrier dynamics in InGaN/GaN nanowires with and without Rh/Cr_2O_3 nanoparticle decoration have been investigated using femtosecond transient absorption techniques with excitation at 415 nm and white-light probe (450–700 nm) [32–34].

Furthermore, an efficient visible-light photoelectrochemical photodetector based on a compact In-rich n-InGaN layer activated by p-Cu_2O microcrystals operating as a photoanode in the self-powered mode was illustrated. The excellent performance was attributed to maximized photocarrier separation in the built-in electric field of the internal p–n junction for fully depleted Cu_2O microcrystals with maximized height and the planar geometry, guaranteeing unhindered diffusion of the electrolyte to and from the photoanode surface [35].

Doping reduces the indium atom composition, the aggregation of In–In and induces the deep energy level. This greatly decreases the defects and improves the valence band potential of InGaN nanorods [36]. Composites based on indium oxide containing different amounts of zinc oxide were synthesized by hydrothermal and impregnation methods. The phase composition, structure, and specific surface of the obtained composites are studied by various physicochemical methods. It was indicated that the method of formation has a significant effect on the structural characteristics of the composites, which in turn leads to the implementation of various conduction mechanisms [37–39].

In this paper, we propose feasible ternary alloys of gallium indium phosphide (GaInP) and Indium gallium arsenide (GaInAs), which are doped with silicon, zinc, or silver. We carried out molecular modelling considering the geometrical parameters of doping atoms on the surface of GaInP and GaInAs, and the absorption status and current charge density of the solar cells were studied. Moreover, the effect of a relative chemical shift between GaInP, GaInAs, and their derivatives and doped heteroclusters of the solar cell was also investigated [40–42].

Meanwhile, it is feasible for the economic growth of GaP epi-layer using silicon substrates because of its high lattice match with silicon. GaP nanowires can be synthesized by the SLS method and show a positive open-circuit photovoltage [43].

The GaP–ZnO core–shell nanowire (NW) heterojunction integrated on top of a multi-junction solar cell can extend its spectral sensitivity region toward shorter wavelengths, enhance the photon absorption, and reduce the surface light reflection [44].

This study aims to model and identify optimal dopants for achieving structural pliability and favorable electronic properties in hybrid III–V semiconductor architectures.

2. Materials and Methods

The Si-, Zn-, or Ag-doped ternary alloys of GaInP (Figure 1a) and GaInAs (Figure 1a′) as solar cells were calculated within the framework of first-principles calculation based on density functional theory (DFT) (Figure 1b,b′,c,c′,d,d′).

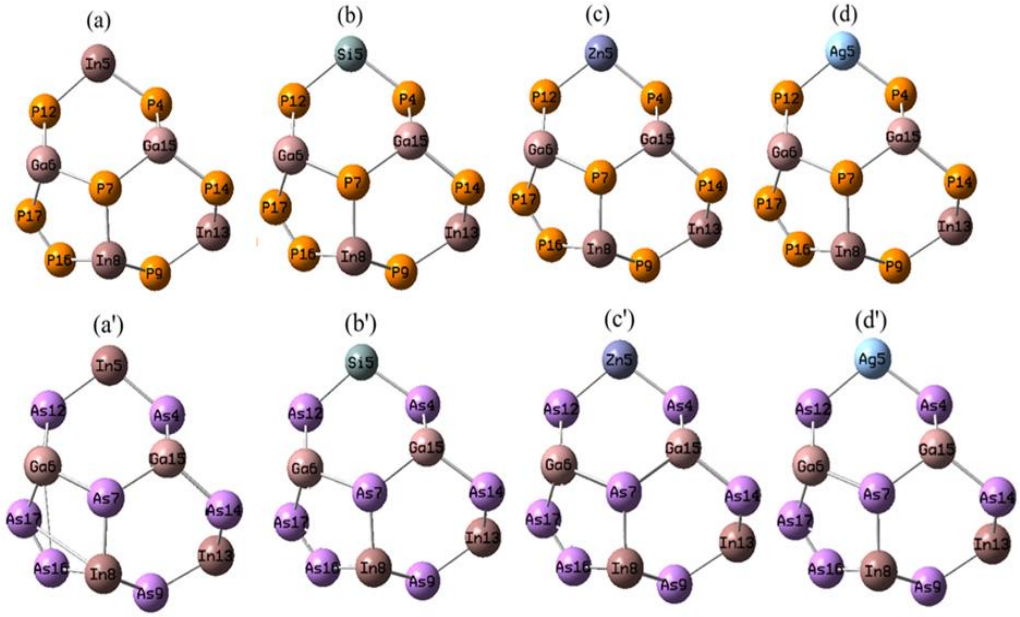

Figure 1. Application of heteroclusters of (a) GaInP, (b) SiGaInP, (c)ZnGaInP, (d) AgGaInP, (a′) GaInAs, (b′) SiGaInAs, (c′) ZnGaInAs, (d′)AgGaInAs for energy storage in solar cells using CAM–B3LYP–D3/6-311+G (d,p) calculation.

3. Results and Discussion

The DFT method presents the electronic density arising from the simple superposition of atomic charges ρ_{SAO}, the density obtained by full solution of the DFT Kohn-Sham equation $\rho_{KS,}$ and the difference of these two:

$$\Delta\rho \equiv \rho_{KS} - \rho_{SAO} \qquad (1)$$

Any superposition of charges of separated atoms has no electric dipole moment; therefore, either Kohn-Sham density ρKS or the density difference Δρ may be used for the calculation of the polarization and the polarization-induced electric field. In principle, the results obtained using both approaches should differ only by an error arising from the intersection of the subtracted separated atom charge by the top and bottom boundaries. The coordinate shift, resulting from the periodic boundary conditions, may affect the magnitude of the dipole obtained from the integration over the simulated volume [45–52].

The rigid potential energy surface using density functional theory [53–58] was performed due to the Gaussian 16 revision C.01 program package [59] and GaussView 6.1 [60]. The coordination input for energy storage on the solar cells has applied 6-311+G (d,p)

and EPR–3 basis sets. The NQR method is related to the multipole expansion in Cartesian coordinates as in equation (2) [61,62].

$$V(r) = V(0) + \left[\left(\frac{\partial V}{\partial x_i}\right)\Big|_0 . \partial x_i\right] + \frac{1}{2}\left[\left(\frac{\partial^2 V}{\partial x_i x_j}\right)\Big|_0 . \partial x_i \partial x_j\right] \quad (2)$$

After that, a simplification of equation (2), there are only the second derivatives related to the identical variable for the potential energy [61,62].

$$U = -\frac{1}{2}\int_{\mathcal{D}} d^3 r\, \rho_r \left[\left(\frac{\partial^2 V}{\partial x_i^2}\right)\Big|_0 . \partial x_i^2\right] = -\frac{1}{2}\int_{\mathcal{D}} d^3 r\, \rho_r \left[\left(\frac{\partial E_i}{\partial x_i}\right)\Big|_0 . \partial x_i^2\right] = -\frac{1}{2}\left(\frac{\partial E_i}{\partial x_i}\right)\Big|_0 . \int_{\mathcal{D}} d^3 r\, [\rho(r) . \partial x_i^2] \quad (3)$$

There are two parameters that must be obtained from NQR experiments: the quadrupole coupling constant, χ, and the asymmetry parameter of the EFG tensor η:

$$\chi = {e^2 Q q_{zz}}/{h} \quad (4)$$

$$\eta = {q_{xx} - q_{yy}}/{q_{zz}} \quad (5)$$

Where q_{ii} are ingredients of the EFG tensor at the quadrupole nucleus are determined in the EFG principal axes system, Q is the nuclear quadrupole moment, e is the proton charge, and h is Planck's constant [63,64].

Solid-state NMR spectroscopy is a technique for characterizing atomic-level structure in solid materials such as powders, single crystals, and amorphous samples and tissues. Solid-state NMR has been successfully used to study metal-organic frameworks (MOFS), batteries, and surfaces of nanoporous materials [65–70].

From the DFT calculations, the chemical shielding (CS) tensors have been attained in the principal axes system for estimating the isotropic chemical-shielding (CSI) and anisotropic chemical-shielding (CSA) [71]:

$$\sigma_{iso} = (\sigma_{11} + \sigma_{22} + \sigma_{33})/3 \quad (6)$$

$$\sigma_{aniso} = \sigma_{33} - (\sigma_{22} + \sigma_{11})/2 \quad (7)$$

Figure 1a,a′,b,b′,c,c′,d,d′ shows the process of energy storage on heteroclusters of GaInP, SiGaInP, ZnGaInP, AgGaInP, GaInAs, SiGaInAs, ZnGaInAs, AgGaInAs, which is varied to maximize the absorption in the active region. Further, we optimized the structural parameters of ternary alloys of GaInP or GaInAs, which are doped with silicon, zinc, or silver, towards the formation of heteroclusters of SiGaInP, ZnGaInP, AgGaInP, SiGaInAs, ZnGaInAs, and AgGaInAs for obtaining the highest short-circuit current density in these solar cells [72–74].

3. Results and Discussion

3.1. Theory of nuclear quadrupole resonance (NQR).

The NQR frequencies have been measured for ternary alloys of GaInP, GaInAs, and doped heteroclusters of SiGaInP, ZnGaInP, AgGaInP, SiGaInAs, ZnGaInAs, and AgGaInAs (Tables 1 and 2). In this research work, the electric potential as the quantity of work energy

through carrying over the electric charge from one position to another position in the essence of the electric field has been evaluated for GaInP, SiGaInP, ZnGaInP, AgGaInP, GaInAs, SiGaInAs, ZnGaInAs, and AgGaInAs heteroclusters (Tables 1 and 2).

Table 1. The electric potential (Ep/a.u.) and Bader charge (Q/coulomb) through NQR calculation for heteroclusters of GaInP, SiGaInP, ZnGaInP, and AgGaInP.

GaInP			SiGaInP			ZnGaInP			AgGaInP		
Atom	**Q**	**E_p**	**Atom**	**Q**	**E_p**	**Atom**	**Q**	**E_p**	**Atom**	**Q**	**E_p**
Ga1	0.1026	–1.2118	Ga1	0.1047	–1.2039	Ga1	0.1148	–1.2146	Ga1	0.1059	–1.2090
P2	0.1169	–2.7295	P2	–0.1107	–2.7218	P2	–0.1356	–2.7355	P2	–0.1198	–2.7340
In3	0.1511	–1.0479	In3	0.1546	–1.0333	In3	0.1158	–1.0632	In3	0.0663	–1.0634
P4	–0.1682	–2.7542	P4	–0.2542	–2.7455	P4	–0.2580	–2.7767	P4	–0.1137	–2.7460
In5	0.1545	–1.0835	Si5	0.1528	–1.9191	Zn5	0.3590	–16.1738	Ag5	0.0475	–17.8017
Ga6	0.0654	–1.2180	Ga6	0.0674	–1.2054	Ga6	0.0784	–1.2197	Ga6	0.0585	–1.2241
P7	–0.1131	–2.7334	P7	–0.1063	–2.7257	P7	–0.1255	–2.7349	P7	–0.1205	–2.7360
In8	0.1981	–1.0517	In8	0.1988	–1.0448	In8	0.1568	–1.0594	In8	0.1334	–1.0522
P9	–0.0045	–2.7509	P9	–0.0256	–2.7486	P9	–0.0082	–2.7556	P9	–0.0123	–2.7489
P10	–0.0457	–2.8011	P10	–0.0490	–2.7920	P10	–0.0176	–2.7798	P10	–0.0188	–2.7820
Ga11	0.0537	–1.2379	Ga11	0.0734	–1.2309	Ga11	0.0613	–1.2379	Ga11	0.0849	–1.2351
P12	–0.1081	–2.7286	P12	–0.1475	–2.7020	P12	–0.1734	–2.7518	P12	0.0125	–2.7267
In13	–0.1298	–1.1006	In13	–0.0870	–1.0914	In13	–0.1605	–1.0991	In13	–0.1669	–1.0895
P14	–0.0660	–2.7964	P14	–0.0656	–2.7891	P14	–0.0507	–2.7938	P14	–0.0459	–2.7875
Ga15	0.0387	–1.2407	Ga15	0.0659	–1.2331	Ga15	0.0540	–1.2400	Ga15	0.0854	–1.2357
P16	–0.0310	–2.6480	P16	–0.0352	–2.6338	P16	–0.0302	–2.6547	P16	–0.0229	–2.6434
P17	0.0192	–2.6501	P17	0.0636	–2.6311	P17	0.0197	–2.6582	P17	0.0265	–2.6448

Table 2. The electric potential (Ep/a.u.) and Bader charge (Q/coulomb) through NQR calculation for heteroclusters of GaInAs, SiGaInAs, ZnGaInAs, and AgGaInAs.

GaInAs			SiGaInAs			ZnGaInAs			AgGaInAs		
Atom	**Q**	**E_p**	**Atom**	**Q**	**E_p**	**Atom**	**Q**	**E_p**	**Atom**	**Q**	**E_p**
Ga1	0.0418	–1.2092	Ga1	0.0258	–1.1973	Ga1	0.0096	–1.2084	Ga1	0.0241	–1.2016
As2	–0.0748	–2.4958	As2	–0.0553	–2.4882	As2	–0.0664	–2.4990	As2	–0.0559	–2.4995
In3	0.1217	–1.0352	In3	0.1032	–1.0220	In3	0.0818	–1.0426	In3	0.0068	–1.0478
As4	–0.1314	–2.5202	As4	–0.2009	–2.5168	As4	–0.2128	–2.5473	As4	–0.0691	–2.5131
In5	0.1363	–1.0687	Si5	0.1067	–1.9233	Zn5	0.3460	–16.1600	Ag5	0.0406	–17.8014
Ga6	0.0244	–1.2045	Ga6	0.0008	–1.198	Ga6	0.0116	–1.2141	Ga6	–0.0015	–1.2160
As7	–0.0609	–2.4974	As7	–0.0445	–2.4916	As7	–0.0689	–2.5018	As7	–0.0612	–2.5010
In8	0.1452	–1.0427	In8	0.1400	–1.0302	In8	0.1141	–1.0372	In8	0.0703	–1.0363
As9	0.0242	–2.5266	As9	0.0209	–2.5121	As9	0.0661	–2.5138	As9	0.0465	–2.5096
As10	0.0170	–2.5554	As10	0.0039	–2.5551	As10	0.0108	–2.5620	As10	0.0384	–2.5482
Ga11	–0.0086	–1.2263	Ga11	0.0066	–1.2226	Ga11	–0.0173	–1.2331	Ga11	0.0140	–1.2257
As12	–0.0527	–2.4868	As12	–0.0710	–2.4699	As12	–0.1167	–2.5155	As12	0.0668	–2.4984
In13	–0.2405	–1.0817	In13	–0.1729	–1.0715	In13	–0.2810	–1.0799	In13	–0.2954	–1.0708
As14	–0.0078	–2.5582	As14	–0.0191	–2.5561	As14	0.0098	–2.5512	As14	0.0203	–2.5500
Ga15	–0.0170	–1.2257	Ga15	0.0005	–1.2239	Ga15	–0.0098	–1.2307	Ga15	0.0190	–1.2255
As16	0.0041	–2.3759	As16	0.0334	–2.3516	As16	0.0425	–2.3646	As16	0.0377	–2.3629
As17	0.0790	–2.3757	As17	0.1218	–2.3508	As17	0.0805	–2.3693	As17	0.0984	–2.3679

The atoms of P/As10, P/As14 extracted from ternary heteroclusters of GaInP and GaInAs have exhibited the fluctuation in the range of -1.5 to +1 coulomb with an average electric potential of about -20 a.u. Then, the hetero clusters of SiGaInP and SiGaInAs with active atoms of P/As10, P/As14, P/As16, P/As17 have been oscillated in the range of -1.5 to +1 coulomb with an average electric potential of about –20 a.u. However, in two hereto-clusters of ZnGaInP and ZnGaInAs, the atoms of P/As10, P/As14, P/As14, P/As16, P/As17 have been considered as fluctuating atoms between -1.5 and +1 coulomb with an average electric potential of about -23 a.u. In fact, by doping transition metals of Zn and Ag into GaInP and GaInAs, the electric potential extracted from NQR calculations grows. Therefore, it can be proposed that doped alloys of SiGaInP, ZnGaInP, AgGaInP, SiGaInAs, ZnGaInAs, and AgGaInAs might augment the ability of GaInP and GaInAs in solar cells for energy storage.

The two heteroclusters of ZnGaInP/As and AgGaInP/As, with the fluctuations of In, Ga, P, As, and transition metals of Zn, Ag, have indicated the same sensitivity of electric potential. On the other hand, the electrical conductivity based on NQR parameters in Tables 1 and 2 can be enhanced with doping Zn or Ag. Therefore, it can be considered that zinc and silver atoms in the functionalized ZnGaInP/As and AgGaInP/As might have more impressive sensitivity for accepting electrons in the process of energy adsorption mechanism.

3.2. Analysis of nuclear magnetic resonance spectra.

Based on the resulting amounts, nuclear magnetic resonance (NMR) spectra of GaInP, SiGaInP, ZnGaInP, AgGaInP, GaInAs, SiGaInAs, ZnGaInAs, and AgGaInAs heteroclusters as the potential molecules for energy storage can unravel the efficiency of these complexes in solar cells. The NMR data of isotropic (σiso) and anisotropic shielding tensors (σaniso) of a ternary alloy of GaInP, GaInAs, and doped heteroclusters of SiGaInP, ZnGaInP, AgGaInP, SiGaInAs, ZnGaInAs, and AgGaInAs have been computed by the Gaussian 16 revision C.01 program package [40] and are shown in Tables 3 and 4. NMR data have reported notable amounts for GaInP, SiGaInP, ZnGaInP, AgGaInP, GaInAs, SiGaInAs, ZnGaInAs, and AgGaInAs heteroclusters. The notable fragile signal intensity close to the parallel edge of the nanocluster sample might be owing to indium or gallium binding, induced non-spherical distribution of GaInP and GaInAs heteroclusters. It exhibited the same tendency of shielding for indium or gallium; however, a considerable deviation exists from doping atoms of silicon, zinc, and silver as electron acceptors on the surface of GaInP and GaInAs heteroclusters (Tables 3 and 4).

Table3. Data of NMR shielding tensors (ppm) for selected atoms of heteroclusters containing GaInP, SiGaInP, ZnGaInP, and AgGaInP.

GaInP			SiGaInP			ZnGaInP			AgGaInP		
Atom	**σ_{iso}**	**σ_{aniso}**	**Atom**	**σ_{iso}**	**σ_{aniso}**	**Atom**	**σ_{iso}**	**σ_{aniso}**	**Atom**	**σ_{iso}**	**σ_{aniso}**
Ga1	2.9912	16.4084	Ga1	14.7085	140.2988	Ga1	5.7833	14.5749	Ga1	3.7750	34.4763
P2	16.2010	40.6634	P2	68.4834	625.8891	P2	30.2094	47.7035	P2	22.9294	18.0919
In3	3.1564	15.8887	In3	131.7170	427.4682	In3	7.9646	11.9775	In3	3.6760	11.4878
P4	22.7075	60.8319	P4	804.6769	1389.8580	P4	36.5989	41.5291	P4	47.5503	27.4761
In5	10.9969	13.8506	Si5	2860.3818	5164.8465	Zn5	9.3438	226.6506	Ag5	393.5721	558.6332
Ga6	1.2904	24.4243	Ga6	267.4956	566.4396	Ga6	9.2207	17.2757	Ga6	2.9683	6.6546
P7	17.2864	58.4028	P7	16.2609	542.0997	P7	25.2067	38.3781	P7	24.0390	19.4948
In8	4.9301	14.9211	In8	9.0080	97.6623	In8	4.7382	12.3749	In8	8.3272	23.2560
P9	28.8631	25.4405	P9	91.8204	246.9075	P9	37.5249	47.2443	P9	58.9997	117.4414
P10	30.7698	116.3719	P10	503.5063	1881.0068	P10	8.5079	171.6037	P10	60.6719	105.9426
Ga11	6.3168	13.0068	Ga11	50.1587	319.1833	Ga11	7.0744	9.5749	Ga11	0.2429	18.3864
P12	9.1231	22.0187	P12	884.9371	1426.2068	P12	14.2417	29.1589	P12	75.2296	156.3703
In13	5.6051	14.0973	In13	58.6594	165.8298	In13	7.9784	16.4409	In13	8.8481	26.4861
P14	58.3719	117.9195	P14	322.0308	1477.9439	P14	51.7048	178.1570	P14	60.3844	116.8811
Ga15	6.1193	14.0998	Ga15	115.3250	362.1296	Ga15	5.7509	10.6229	Ga15	1.2247	19.7986
P16	17.2493	20.2584	P16	75.5403	269.6551	P16	13.3250	15.1974	P16	52.6745	55.9966
P17	16.5831	31.6549	P17	111.5741	550.4411	P17	9.9093	27.4979	P17	13.2274	25.9349

Table 4. Data of NMR shielding tensors (ppm) for selected atoms of heteroclusters containing GaInAs, SiGaInAs, ZnGaInAs, and AgGaInAs.

GaInAs			SiGaInAs			ZnGaInAs			AgGaInAs		
Atom	**σ_{iso}**	**σ_{aniso}**	**Atom**	**σ_{iso}**	**σ_{aniso}**	**Atom**	**σ_{iso}**	**σ_{aniso}**	**Atom**	**σ_{iso}**	**σ_{aniso}**
Ga1	0.3074	22.0861	Ga1	0.0792	15.9341	Ga1	0.6750	21.1703	Ga1	0.7520	19.8593
As2	29.8236	19.6313	As2	25.3146	28.6917	As2	23.1833	28.7591	As2	29.3266	14.1258
In3	6.9570	15.2904	In3	4.0747	36.0498	In3	9.8905	16.7811	In3	5.4711	11.9363
As4	31.1679	42.1877	As4	26.3934	58.6309	As4	37.8469	30.5219	As4	34.4168	33.3078
In5	6.5331	26.0498	Si5	82.2563	134.8817	Zn5	28.1128	258.0039	Ag5	264.0270	198.3803
Ga6	4.9931	21.3464	Ga6	1.0019	48.1536	Ga6	11.0560	27.7590	Ga6	3.9803	10.8326
As7	29.2555	20.4417	As7	25.7353	29.6306	As7	37.7734	43.6597	As7	29.3101	14.7364

In8	3.2540	15.6435	In8	3.7465	12.1451	In8	10.0028	17.3503	In8	4.9978	14.0723
As9	33.1441	18.2773	As9	33.2210	29.1774	As9	37.1966	37.6456	As9	34.0167	16.5118
As10	1.5355	38.3636	As10	4.2091	50.1160	As10	87.3312	281.8346	As10	7.5991	55.2786
Ga11	8.5234	16.2496	Ga11	9.7332	22.7859	Ga11	12.4382	26.1392	Ga11	4.9066	9.7615
As12	20.4792	16.4775	As12	4.8271	41.5559	As12	16.7441	28.0545	As12	9.4031	63.4163
In13	13.9073	6.6538	In13	3.6415	12.8873	In13	10.8811	28.1587	In13	3.2084	14.9917
As14	5.2686	38.8713	As14	0.8467	70.3439	As14	16.6354	217.0360	As14	7.1376	59.5777
Ga15	8.8580	15.0711	Ga15	9.4986	22.0994	Ga15	4.8167	21.5119	Ga15	4.0903	10.4577
As16	19.6123	28.1556	As16	16.1567	18.0408	As16	17.2297	24.7023	As16	34.4048	21.6306
As17	16.0551	27.6943	As17	19.0565	9.8546	As17	1.8169	24.5890	As17	18.6066	19.6882

The yield of electromagnetic shifting can be directed by atoms of P/As10 and P/As14 extracted from ternary hereto clusters of GaInP and GaInAs. Tables 3 and 4 show that the intensity for energy storage can be enhanced in SiGaInP and SiGaInAs due to oscillating chemical shielding in P/As10, P/As14, P/As16, and P/As17 atoms. The atoms of P/As10, P/As4, P/As14, P/As16, and P/As17 have indicated the fluctuation in chemical shielding for ZnGaInP/As and AgGaInP/As. So, it can be observed that doped heteroclusters of SiGaInP/As, ZnGaInP/As, and AgGaInP/As might ameliorate the capability of GaInP/As in solar cells for energy storage.

3.3. Insight into infrared spectroscopy and thermochemistry.

The infrared spectroscopy (IR) has been performed for the ternary alloy of GaInP, GaInAs, and doped heteroclusters of SiGaInP, ZnGaInP, AgGaInP, SiGaInAs, ZnGaInAs, and AgGaInAs (Figure 2a,a′,b,b′,c,c′,d,d′). Figure 2(a,b,c,d) indicates the fluctuation of frequency between 400–2200 cm^{-1} for GaInP, SiGaInP, ZnGaInP, and AgGaInP with sharp peaks around 800 and 2200 cm^{-1}. Furthermore, the fluctuation of frequency between 400–1600 cm^{-1} for GaInAs, SiGaInAs, ZnGaInP, and AgGaInP with sharp peaks around 600 and 1500 cm^{-1} has been found (Figure 2a ′,b′,c′,d′).

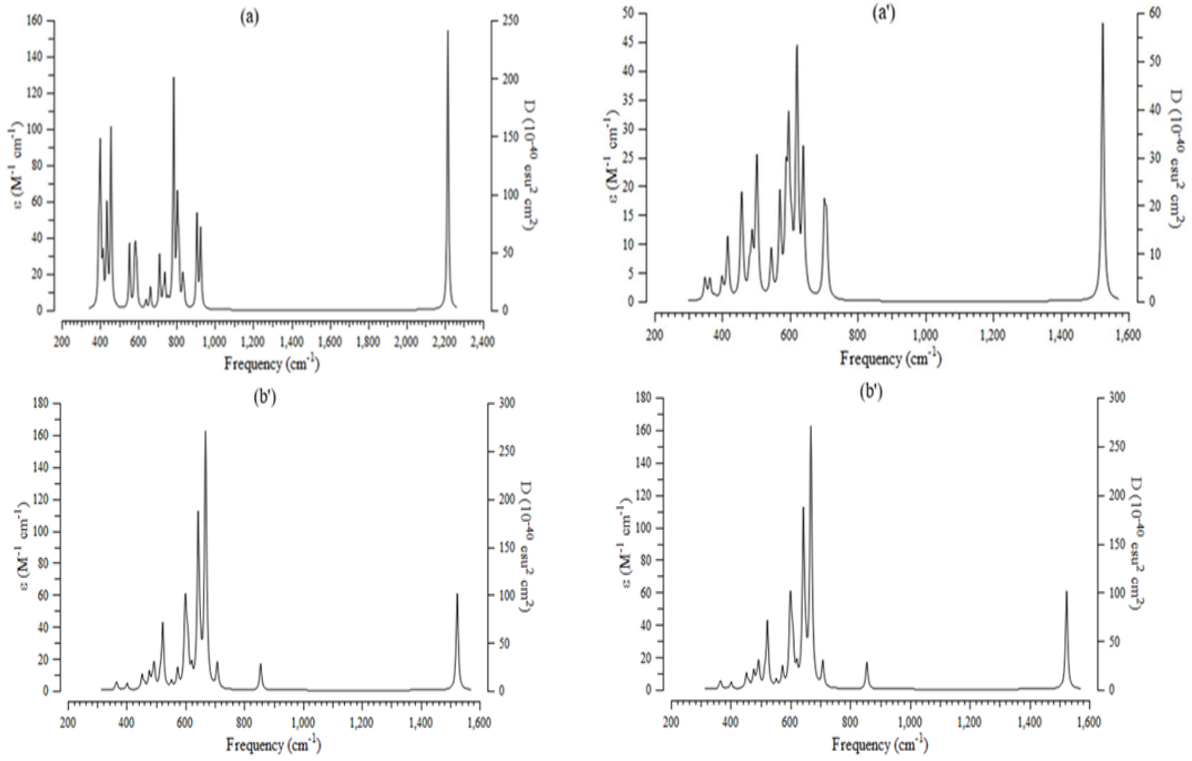

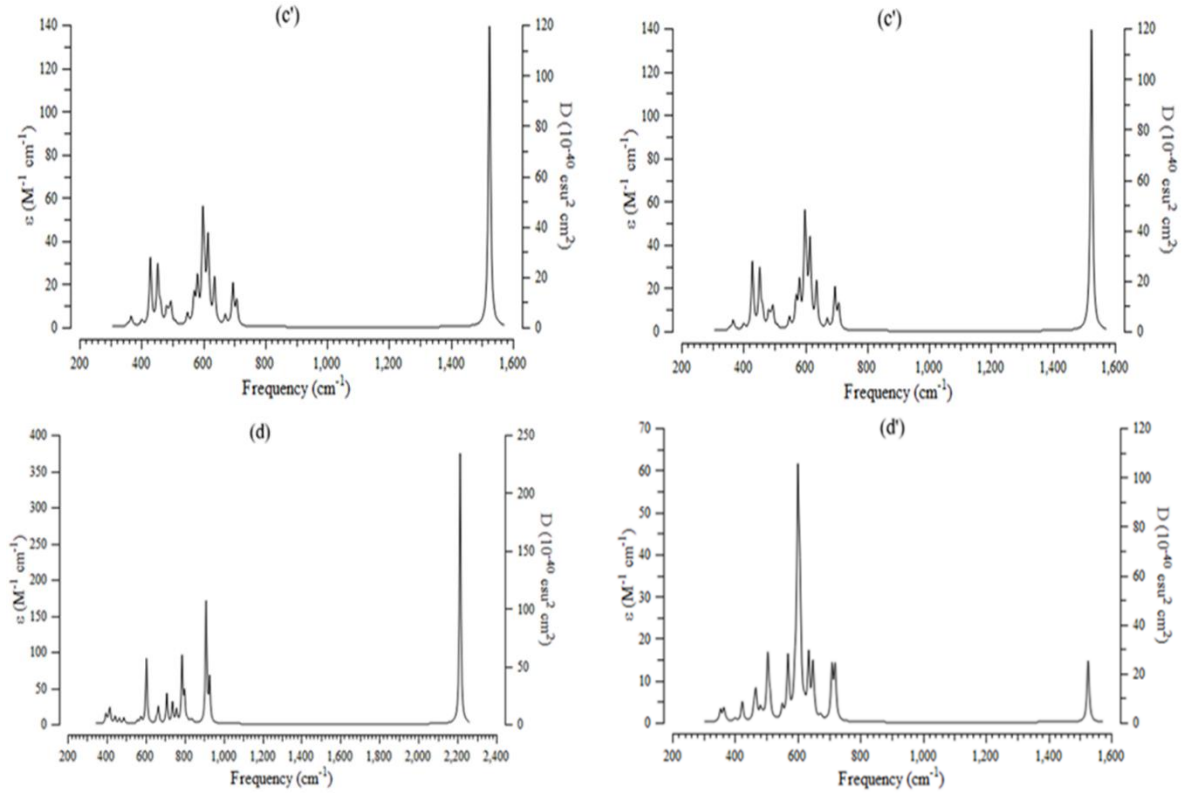

Figure 2. The frequency (cm^{-1}) changes through the IR spectra for heteroclusters of **(a)** GaInP; **(a′)** GaInAs; **(b)** SiGaInP; **(b′)** SiGaInAs; **(c)** ZnGaInP; **(c′)** ZnGaInAs; **(d)** AgGaInP; **(d′)** AgGaInAs.

Energy storage with heteroclusters has been described as a framework for overcoming clusters related to SiGaInP/As, ZnGaInP/As, and AgGaInP/As at high frequencies. This property makes these heteroclusters potentially advantageous for certain high-frequency applications requiring solar cells for energy storage. The advantages of silicon, zinc, and silver over gallium indium phosphide and gallium indium arsenide include their higher electron and hole mobility, which allows silver-doped devices to operate at higher frequencies than silicon- and zinc-doped devices.

Table 5, based on thermodynamic specifications, concluded that heteroclusters of GaInP, SiGaInP, ZnGaInP, AgGaInP, GaInAs, SiGaInAs, ZnGaInAs, and AgGaInAs might be a more efficient structure for energy storage in solar cells. Thermodynamic parameters of heteroclusters of SiGaInP, ZnGaInP, AgGaInP, SiGaInAs, ZnGaInAs, and AgGaInAs have been assigned through doping of ternary alloys of GaInP and GaInAs with Si, Zn, and Ag towards the formation of heteroclusters (Table 5).

Table 5. HOMO(eV), LUMO (eV), energy gap ($\Delta E=E_{LUMO}-E_{HOMO}$ /eV), dipole moment (D/debye), Stability energy (ΔE^{o}_{f} /kcal/mol), thermal entahlpy (ΔH^{o}_{f} /kcal/mol), gibbs free energy (ΔG^{o}_{f} /kcal/mol), entropy(S^{o}_{ads}/cal/Kmol), $E^{o}_{atom\text{-}doping}$ (kcal/mol) of GaInP, SiGaInP, ZnGaInP, AgGaInP, GaInAs, SiGaInAs, ZnGaInAs, AgGaInAs using CAM–B3LYP–D3/6-311+G (d,p) calculation.

Compound	E_{HOMO}	E_{LUMO}	ΔE	D	$\Delta E^{o}_{f}\times10^{-3}$	$\Delta H^{o}_{f}\times10^{-3}$	$\Delta G^{o}_{f}\times10^{-3}$	S^{o}_{ads}	$E^{o}_{atom\text{-}doping}$
GaInP	–4.7920	–4.1232	0.6688	8.2065	–44.7046	–44.7041	–44.7324	94.915	-
SiGaInP	–4.5004	–3.5134	0.9860	9.2277	–46.0130	–46.0124	–46.0399	92.431	–1.3084
ZnGaInP	–4.1434	–3.3940	0.7495	7.1636	–84.6627	–84.6621	–84.6898	93.069	–39.9581
AgGaInP	–4.7693	–3.0462	1.7231	7.0827	–134.9798	–134.9792	–135.0074	94.694	–90.2752
GaInAs	–4.5382	–4.2658	0.2724	6.8245	–41.9156	–41.9150	–41.9452	101.109	-
SiGaInAs	–4.5016	–3.2143	1.2872	8.4976	–43.2327	–43.2321	–43.2615	98.570	–1.3171
ZnGaInAs	–4.1435	–3.3940	0.7495	7.1003	–81.8811	–81.8805	–81.9102	99.358	–39.9655
AgGaInAs	–4.4964	–3.1856	1.3108	6.3828	–132.1937	–132.1931	–132.2232	100.844	–90.2781

The adsorption efficiency of GaInP, SiGaInP, ZnGaInP, AgGaInP, GaInAs, SiGaInAs, ZnGaInAs, AgGaInAs based on dipole moment has been evaluated by the 〖ΔG〗_f^o. The changes of Gibbs free energy versus dipole moment could detect the maximum efficiency of AgGaInP and AgGaInAs heteroclusters for energy storage in the solar cells through 〖ΔG〗_(f, AgGaInP)^o=–134.9792×103 kcal/mol and 〖ΔG〗_(f, AgGaInAs)^o=–132.1931×10 kcal/mol, respectively (Table 5 and Figure 3). Moreover, In GaInP and GaInAs, the photo-excited electrons and holes are strongly bounded by the excitons because of their large exciton binding energy as Eo AgGaInX> Eo ZnGaInX> Eo SiGaInX (X=P or As) due to their efficient exciton dissociation (Table 5).

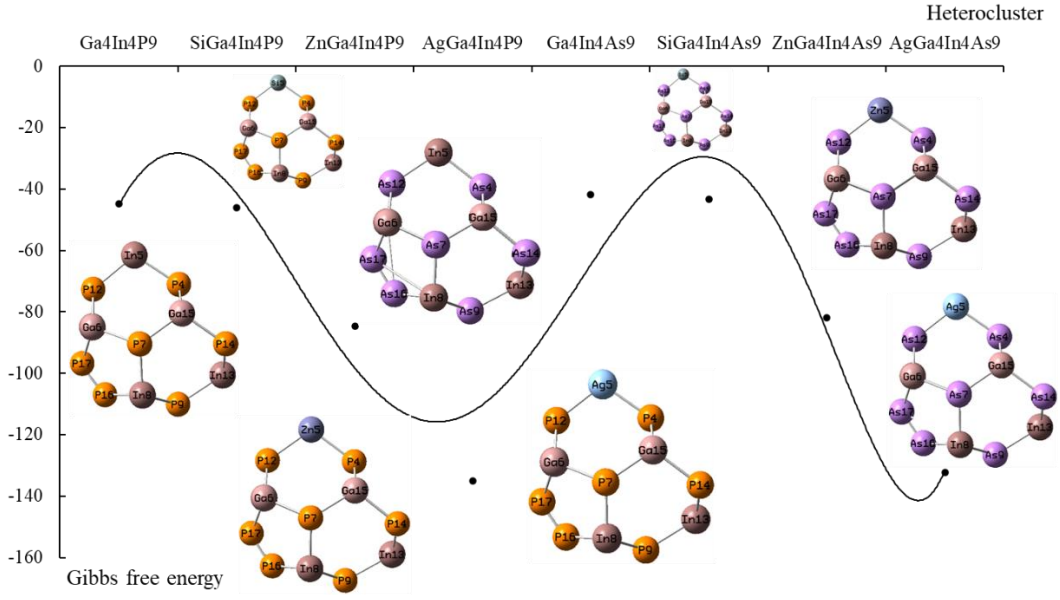

Figure 3. Changes of Gibbs free energy (kcal/mol) for heteroclusters of GaInP, GaInAs, SiGaInP, SiGaInAs, ZnGaInP, ZnGaInAs, AgGaInP, and AgGaInAs.

Besides, the intermolecular orbital overlap integral is important in the illustration of intermolecular charge transfer, which can compute HOMO-HOMO and LUMO-LUMO overlap integrals between Si, Zn, Ag atoms, and GaInP/As nanostructure (Table 5). The wavefunction level we used was CAM–B3LYP–D3/6–311+G(d,p), which corresponds to HOMO and LUMO, respectively (Table 5). Therefore, ELUMO (a.u.), ELUMO (a.u.), and the local bandgap energies (ΔE/a.u.) and immobile charges induced by polarization discontinuity are simultaneously controlled throughout the structures, and optimized band profiles are eventually achieved for GaInP, SiGaInP, ZnGaInP, AgGaInP, GaInAs, SiGaInAs, ZnGaInAs, and AgGaInAs nanoclusters (Table 5).

The solar cells formed by GaInP, SiGaInP, ZnGaInP, AgGaInP, GaInAs, SiGaInAs, ZnGaInAs, and AgGaInAs feature a hierarchical structure with the electron donor/acceptor layer sandwiched by anode and cathode, which raises the importance of controlling the molecular crystal orientation, domain size, and vertical distribution to facilitate the charge collection at electrodes. Doping obviously reduces the indium atom composition, the aggregation of In–In and induces the deep energy level. This greatly decreases the defects and improves the valence band potential of GaInP and GaInAs nanorods. In this paper, we have demonstrated that the ternary semiconductors of gallium indium phosphide and gallium indium arsenide can lead to a significant absorption enhancement in a broad spectral range of incident light in the presence of silicon, zinc, or silver. This efficient doping strategy not only bridges

the gaps of heteroatom-doped GaInP or GaInAs-based photoelectrodes but also can provide deep insights into controlling the electronic structure for enhanced solar conversion efficiency [75–77]. Indium phosphide quantum dots represent a promising solution to these challenges; unfortunately, they typically suffer from low inherent emissivity resulting from charge carrier trapping. Strategies to improve the emissive characteristics of indium phosphide often involve zinc incorporation into or onto the core itself and the fabrication of core/shell heterostructures. InP clusters are high-fidelity platforms for studying processes such as cation exchange and surface doping with exogenous ions, since these clusters are used as single-source precursors for quantum dot synthesis.

4. Conclusions

In summary, we explored and proposed high-efficiency solar cells based on GaInP and GaInAs transducers with an isoelectronic (Si, Zn, Ag)-doped layer. Energy grabbing on the heteroclusters of SiGaInP, ZnGaInP, AgGaInP, SiGaInAs, ZnGaInAs, and AgGaInAs in solar cells was investigated by first-principles calculations. The effect of a relative chemical shift between GaInP, GaInAs, and doped heteroclusters of the solar cell was also investigated. Thermodynamic parameters have constructed a detailed molecular model for atom–atom interactions and a distribution of point charges which can be utilized to reproduce the polarity of the solid material and the adsorbing molecules. In GaInP and GaInAs, the photo-excited electrons and holes are strongly bound by the excitons because of their large exciton binding energy as Eo AgGaInX> Eo ZnGaInX> Eo SiGaInX (X=P or As) due to their efficient exciton dissociation. The two heteroclusters of ZnGaInP/As and AgGaInP/As, with the fluctuations of In, Ga, P, As, and transition metals of Zn, Ag, have indicated the same sensitivity of electric potential. On the other hand, the electrical conductivity based on NQR parameters can be enhanced by doping Zn or Ag. The advantages of silver over gallium indium phosphide and gallium indium arsenide include its higher electron and hole mobility, allowing silver doping devices to operate at higher frequencies than silicon and zinc doping devices through 〖ΔG〗_(f, AgGaInP)^o=–134.9792×103 kcal/mol and 〖ΔG〗_(f, AgGaInAs)^o=–132.1931×103 kcal/mol, respectively. Thus, it should be explored for its unique properties, such as its ability to increase energy storage, which could lead to advancements in solar cells. This work demonstrates an effective way for boosting the performance of GaInP and GaInAs nanocages and Si-/Zn-/Ag/Ag-doped derivatives cells, which may promote the application of nuclear micro-batteries in extreme environments.

Author Contributions

Conceptualization, F.M.; methodology, F.M.; software F.M.; validation, F.M.; formal analysis, F.M.; investigation, F.M.; resources, F.M.; data curation, F.M.; writing—original draft preparation, F.M.; writing—review and editing, F.M.; visualization, F.M.; supervision, F.M.; project administration, F.M.; funding acquisition, F.M. The author has read and agreed to the published version of the manuscript.

Institutional Review Board Statement

Not applicable.

Informed Consent Statement

Not applicable.

Data Availability Statement

Data supporting the findings of this study are available upon reasonable request from the corresponding author.

Funding

This research received no funding.

Acknowledgments

The author is grateful to Kastamonu University for successfully completing this paper and its research.

Conflict of Interest

The author declares no conflict of interest.

References

1. Di Carlo, A. Tuning Optical Properties of GaN-Based Nanostructures by Charge Screening. *phys. stat. sol. (a)* **2001**, *183*, 81-85, https://doi.org/10.1002/1521-396X(200101)183:1<81::AID-PSSA81>3.0.CO;2-N.
2. Arakawa, Y. Progress in GaN-based quantum dots for optoelectronics applications. *IEEE J. Sel. Top. Quantum Electron.* **2002**, *8*, 823-832, https://doi.org/10.1109/JSTQE.2002.801675.
3. Lukin, L.V. Empirical Model of the Charge Carriers' Photogeneration in Organic Solar Cells. *Russ. J. Phys. Chem. B.* **2024**, *17*, 1300-1308, https://doi.org/10.1134/S1990793123060180.
4. Golubkov, M.; Dmitriev, A.; Suvorova, A.; Golubkov, G. Spatial Distribution of the Precipitations of the Intensive Energetic Electron Fluxes into the Ionosphere within the 23rd and 24th Solar Cycles. *Russ. J. Phys. Chem. B.* **2022**, *16*, 537-542, https://doi.org/10.1134/S199079312203006X.
5. Meng, Q.; Lin, Q.; Han, F.; Jing, W.; Wang, Y.; Jiang, Z. A Terahertz Detector Based on Double-Channel GaN/AlGaN High Electronic Mobility Transistor. *Materials* **2021**, *14*, https://doi.org/10.3390/ma14206193.
6. Mollaamin, F.; Monajjemi, M. Effect of Implanted Titanium, Vanadium or Chromium on Boron Nitride Surface for Increasing Carbon Monoxide Adsorption: Designing Gas Sensor for Green Chemistry Future. *Russ. J. Phys. Chem. B.* **2024**, *18*, 1199-1216, https://doi.org/10.1134/S1990793124700519.
7. Monajjemi, M.; Mollaamin, F.; Shahriari, S.; Khalaj, Z.; Sakhaeinia, H.; Alihosseini, A. Interaction of Nano-Boron Nitride Sheets with Electrodes in Lithium Ion Battery for Increasing Voltage and Amperage. *Russ. J. Phys. Chem. B.* **2024**, *18*, 1090-1112, https://doi.org/10.1134/S1990793124700465.
8. Mollaamin, F.; Monajjemi, M. Selectivity and Sensitivity Evaluation of Embedded BN-Nanostructure as a Gas Detector for Air Pollution Scavenging: a Theoretical Study. *Russ. J. Phys. Chem. B.* **2024**, *18*, 1177-1198, https://doi.org/10.1134/s1990793124700507.
9. Amano, H.; Sawaki, N.; Akasaki, I.; Toyoda, Y. Metalorganic vapor phase epitaxial growth of a high quality GaN film using an AlN buffer layer. *Appl. Phys. Lett.* **1986**, *48*, 353-355, https://doi.org/10.1063/1.96549.
10. Mollaamin, F.; Monajjemi, M. Structural, Electromagnetic and Thermodynamic Analysis of Ion Pollutants Adsorption in Water by Gallium Nitride Nanomaterial: a Green Chemistry Application. *Russ. J. Phys. Chem. B.* **2024**, *18*, 533-548, https://doi.org/10.1134/S199079312402012X.
11. Amano, H.; Kito, M.; Hiramatsu, K.; Akasaki, I. P-Type Conduction in Mg-Doped GaN Treated with Low-Energy Electron Beam Irradiation (LEEBI). *Jpn. J. Appl. Phys.* **1989**, *28*, L2112, https://doi.org/10.1143/JJAP.28.L2112.

12. Amano, H.; Asahi, T.; Akasaki, I. Stimulated Emission Near Ultraviolet at Room Temperature from a GaN Film Grown on Sapphire by MOVPE Using an AlN Buffer Layer. *Jpn. J. Appl. Phys.* **1990**, *29*, L205, https://doi.org/10.1143/JJAP.29.L205.
13. Akasaki, I.; Amano, H.; Sota, S.; Sakai, H.; Tanaka, T.; Koike, M. Stimulated Emission by Current Injection from an AlGaN/GaN/GaInN Quantum Well Device. *Jpn. J. Appl. Phys.* **1995**, *34*, L1517, https://doi.org/10.7567/JJAP.34.L1517.
14. Kodama, M.; Sugimoto, M.; Hayashi, E.; Soejima, N.; Ishiguro, O.; Kanechika, M.; Itoh, K.; Ueda, H.; Uesugi, T.; Kachi, T. GaN-Based Trench Gate Metal Oxide Semiconductor Field-Effect Transistor Fabricated with Novel Wet Etching. *Appl. Phys. Express* **2008**, *1*, 021104, https://doi.org/10.1143/APEX.1.021104.
15. Wraback, M.; Shen, H.; Carrano, J.C.; Li, T.; Campbell, J.C.; Schurman, M.J.; Ferguson, I.T. Time-resolved electroabsorption measurement of the electron velocity-field characteristic in GaN. *Appl. Phys. Lett.* **2000**, *76*, 1155-1157, https://doi.org/10.1063/1.125968.
16. Bashirov, R.J. QUALITY CONTROL METHODS AND MODELS OF POLYMER COMPOSITE MATERIALS. *Adv. Phys. Res.* **2024**, *6*, 90-99, https://doi.org/10.62476/apr62.90.
17. Utamuradova, S.B. X-RAY SPECTROSCOPY OF SILICON DOPED WITH GERMANIUM ATOMS. *Adv. Phys. Res.* **2024**, *6*, 211-218, https://doi.org/10.62476/apr63211.
18. Utamuradova, S.; Rakhmanov, D.; Tuan, P.L.; Doroshkevich, A.; Sh, R.; Isayev, R.; Abiyev, A.; Rakhmanov, D. STUDYING THE INFLUENCE OF PROTON IRRADIATION ON THE DISTRIBUTION PROFILE OF Pt AND Cr IN SURFACE LAYERS n-Si<Pt>, n-Si<Cr> USING ELLIPSOMETRIC SPECTROSCOPY. *Adv. Phys. Res.* **2024**, *6*, 83-89, https://doi.org/10.62476/apr62.83.
19. Abdullayeva, L.K. INVESTIGATION OF THE ROLE OF METAL IN NON-ALLOY METAL-SEMICONDUCTOR (Si) CONTACT. *New Mater. Comp. Appl.* **2024**, *8*, 135-141, https://doi.org/10.62476/nmca8135.
20. Mollaamin, F.; Monajjemi, M. Corrosion Inhibiting by Some Organic Heterocyclic Inhibitors Through Langmuir Adsorption Mechanism on the Al-X (X = Mg/Ga/Si) Alloy Surface: A Study of Quantum Three-Layer Method of CAM-DFT/ONIOM. *J. Bio- Tribo-Corros.* **2023**, *9*, 33, https://doi.org/10.1007/s40735-023-00751-y.
21. Gochuyeva, A.; Mehdiyeva, A.; Bakhshaliyeva, S. STUDY OF THE EFFECT OF PHOTO QUENCHING OF ELECTRICAL CONDUCTIVITY UNDER THE ACTION OF LIGHT IN POLYMER-FERROCENE COMPOSITES. *New Mater. Compd. Appl.* **2024**, *8*, 87-93, https://doi.org/10.62476/nmca8187.
22. Mollaamin, F. Features of parametric point nuclear magnetic resonance of metals implantation on boron nitride nanotube by density functional theory/electron paramagnetic resonance. *J. Comput. Theor. Nanosci.* **2014**, *11*, 2393-2398, https://doi.org/10.1166/jctn.2014.3653.
23. Zolotarev, K.V.; Mikhailov, A.N.; Nakhod, V.I.; Sanzhakov, M.A.; Tikhonova, E.G.; Mikhailova, M.V. Characterization and in vivo toxicity assay of uncoated silicon nanoparticles. *New Mater. Comp. Appl.* **2022**, *8*, 162-170, https://doi.org/10.62476/nmca82162.
24. Mollaamin, F.; Monajjemi, M. Nanomaterials for Sustainable Energy in Hydrogen-Fuel Cell: Functionalization and Characterization of Carbon Nano-Semiconductors with Silicon, Germanium, Tin or Lead through Density Functional Theory Study. *Russ. J. Phys. Chem. B.* **2024**, *18*, 607-623, https://doi.org/10.1134/S1990793124020271.
25. Mollaamin, F.; Mohammadi, S.; Khalaj, Z.; Monajjemi, M. Computational Modelling of Boron Nitride Nanosheet for Detecting and Trapping of Water Contaminant. *Russ. J. Phys. Chem. B.* **2024**, *18*, 67-82, https://doi.org/10.1134/S1990793124010330.
26. Abass, A.; Le, K.Q.; Alù, A.; Burgelman, M.; Maes, B. Dual-interface gratings for broadband absorption enhancement in thin-film solar cells. *Physical Review B* **2012**, *85*, 115449, https://doi.org/10.1103/PhysRevB.85.115449.
27. Chriki, R.; Yanai, A.; Shappir, J.; Levy, U. Enhanced efficiency of thin film solar cells using a shifted dual grating plasmonic structure. *Opt. Express* **2013**, *21*, A382-A391, https://doi.org/10.1364/OE.21.00A382.
28. Mollaamin, F. Alkali Metals Doped on Tin-Silicon and Germanium-Silicon Oxides for Energy Storage in Hybrid Biofuel Cells: A First-Principles Study. *Russ. J. Phys. Chem. B.* **2025**, *19*, 720–734, https://doi.org/10.1134/S1990793125700393.
29. Mollaamin, F.; Monajjemi, M. Electric and Magnetic Evaluation of Aluminum–Magnesium Nanoalloy Decorated with Germanium Through Heterocyclic Carbenes Adsorption: A Density Functional Theory Study. *Russ. J. Phys. Chem. B.* **2023**, *17*, 658-672, https://doi.org/10.1134/S1990793123030223.

30. Kourchid, K.; Alaya, R.; Bouguila, N.; Abassi, H.; Mbarki, M. Theoretical Predictions of Structural, Electronic, and Optical Properties of α and β Phases of In_2S_3. *Russ. J. Phys. Chem. B.* **2024**, *18*, 37-48, https://doi.org/10.1134/S1990793124010317.
31. Mollaamin, F.; Monajjemi, M. Graphene Embedded with Transition Metals for Capturing Carbon Dioxide: Gas Detection Study Using QM Methods. *Clean Technol.* **2023**, *5*, 403-417. https://doi.org/10.3390/cleantechnol5010020.
32. Asfour, I. Theoretical Study of the Structural Stability, Electronic and Magnetic Properties of Half-Metallic Ferromagnetism Cr_2NbZ (Z = As, Sb). *Russ. J. Phys. Chem. B.* **2024**, *18*, 83-94, https://doi.org/10.1134/S1990793124010032.
33. Pu, Y.-C.; Kibria, M.G.; Mi, Z.; Zhang, J.Z. Ultrafast Exciton Dynamics in InGaN/GaN and Rh/Cr_2O_3 Nanoparticle-Decorated InGaN/GaN Nanowires. *J. Phys. Chem. Lett.* **2015**, *6*, 2649-2656, https://doi.org/10.1021/acs.jpclett.5b00909.
34. Fatemeh, M. Investigating the Treatment of Transition Metals for Ameliorating the Ability of Boron Nitride for Gas Sensing & Removing: A Molecular Characterization by DFT Framework. *Prot. Met. Phys. Chem. Surf.* **2024**, *60*, 1050-1063, https://doi.org/10.1134/S2070205124702502.
35. Zhang, W.; Deng, R.; Luo, M.; Hong, H.; Pan, X.; Nötzel, R. Fast self-powered n-InGaN layer/p-Cu_2O microcrystal visible-light photoelectrochemical photodetector with high photocurrent and responsivity. *AIP Adv.* **2024**, *14*, 045301, https://doi.org/10.1063/5.0202164.
36. Lin, J.; Yu, Y.; Xu, Z.; Gao, F.; Zhang, Z.; Zeng, F.; Wang, W.; Li, G. Electronic engineering of transition metal Zn-doped InGaN nanorods arrays for photoelectrochemical water splitting. *J. Power Sources* **2020**, *450*, 227578, https://doi.org/10.1016/j.jpowsour.2019.227578.
37. Ikim, M.I.; Spiridonova, E.Y.; Gromov, V.F.; Gerasimov, G.N.; Trakhtenberg, L.I. Effect of the Formation Method of ZnO–In_2O_3 Composites on Their Structural Characteristics and Conductivity. *Russ. J. Phys. Chem. B.* **2024**, *18*, 283-288, https://doi.org/10.1134/S199079312401010X.
38. Ikim, M.I.; Spiridonova, E.Y.; Gromov, V.F.; Gerasimov, G.N.; Trakhtenberg, L.I. Effect of the Type of the Crystal Phase of In_2O_3 On Its Conductivity and Sensor Properties in Hydrogen Detection. *Russ. J. Phys. Chem. B.* **2023**, *17*, 774-777, https://doi.org/10.1134/S199079312303003X.
39. Kumawat, U.K.; Kumar, K.; Bhardwaj, P.; Dhawan, A. Indium-rich InGaN/GaN solar cells with improved performance due to plasmonic and dielectric nanogratings. *Energy Sci. Eng.* **2019**, *7*, 2469-2482, https://doi.org/10.1002/ese3.436.
40. Ghosh, A.; Mohammed, O.F.; Bakr, O.M. Atomic-Level Doping of Metal Clusters. *Acc. Chem. Res.* **2018**, *51*, 3094-3103, https://doi.org/10.1021/acs.accounts.8b00412.
41. Bootharaju, M.S.; Kozlov, S.M.; Cao, Z.; Shkurenko, A.; El-Zohry, A.M.; Mohammed, O.F.; Eddaoudi, M.; Bakr, O.M.; Cavallo, L.; Basset, J.-M. Tailoring the Crystal Structure of Nanoclusters Unveiled High Photoluminescence via Ion Pairing. Chem. Mater. **2018**, *30*, 2719-2725, https://doi.org/10.1021/acs.chemmater.8b00328.
42. Negishi, Y.; Igarashi, K.; Munakata, K.; Ohgake, W.; Nobusada, K. Palladium doping of magic gold cluster $Au_{38}(SC_2H_4Ph)_{24}$: formation of $Pd_2Au_{36}(SC_2H_4Ph)_{24}$ with higher stability than $Au_{38}(SC_2H_4Ph)_{24}$. *Chem. Commun.* **2012**, *48*, 660-662, https://doi.org/10.1039/C1CC15765E.
43. Sun, J.; Liu, C.; Yang, P. Surfactant-Free, Large-Scale, Solution–Liquid–Solid Growth of Gallium Phosphide Nanowires and Their Use for Visible-Light-Driven Hydrogen Production from Water Reduction. *J. Am. Chem. Soc.* **2011**, *133*, 19306-19309, https://doi.org/10.1021/ja2083398.
44. Hasenöhrl, S.; Eliáš, P.; Šoltýs, J.; Stoklas, R.; Dujavová-Laurenčíková, A.; Novák, J. Zinc-doped gallium phosphide nanowires for photovoltaic structures. *Appl. Surf. Sci.* **2013**, *269*, 72-76, https://doi.org/10.1016/j.apsusc.2012.09.109.
45. Mollaamin, F.; Monajjemi, M. In Situ Ti-Embedded SiC as Chemiresistive Nanosensor for Safety Monitoring of CO, CO_2, NO, NO_2: Molecular Modelling by Conceptual Density Functional Theory. *Russ. J. Phys. Chem. B.* **2024**, *18*, 49-66, https://doi.org/10.1134/S1990793124010159.
46. Khalili Hadad, B.; Mollaamin, F.; Monajjemi, M. Biophysical chemistry of macrocycles for drug delivery: a theoretical study. *Russ. Chem. Bull.* **2011**, *60*, 238-241, https://doi.org/10.1007/s11172-011-0039-5.
47. Mollaamin, F.; Monajjemi, M. In Silico-DFT Investigation of Nanocluster Alloys of Al-(Mg, Ge, Sn) Coated by Nitrogen Heterocyclic Carbenes as Corrosion Inhibitors. *J. Clust. Sci.* **2023**, *34*, 2901-2918, https://doi.org/10.1007/s10876-023-02436-5.

48. Mollaamin, F.; Monajjemi, M. Graphene-based resistant sensor decorated with Mn, Co, Cu for nitric oxide detection: Langmuir adsorption & DFT method. *Sensor Rev.* **2023**, *43*, 266-279, https://doi.org/10.1108/SR-03-2023-0040.
49. Mollaamin, F.; Shahriari, S.; Monajjemi, M.; Khalaj, Z. Nanocluster of Aluminum Lattice via Organic Inhibitors Coating: A Study of Freundlich Adsorption. *J. Clust. Sci.* **2023**, *34*, 1547-1562, https://doi.org/10.1007/s10876-022-02335-1.
50. Mollaamin, F.; Monajjemi, M. Application of DFT and TD-DFT on Langmuir Adsorption of Nitrogen and Sulfur Heterocycle Dopants on an Aluminum Surface Decorated with Magnesium and Silicon. *Computation* **2023**, *11*, 108. https://doi.org/10.3390/computation11060108
51. Mollaamin, F.; Monajjemi, M. Tailoring and functionalizing the graphitic-like GaN and GaP nanostructures as selective sensors for NO, NO_2, and NH_3 adsorbing: a DFT study. *J. Mol. Model.* **2023**, *29*, 170, https://doi.org/10.1007/s00894-023-05567-8.
52. Mollaamin, F. Competitive Intracellular Hydrogen-Nanocarrier Among Aluminum, Carbon, or Silicon Implantation: a Novel Technology of Eco-Friendly Energy Storage using Research Density Functional Theory. *Russ. J. Phys. Chem. B.* **2024**, *18*, 805-820, https://doi.org/10.1134/S1990793124700131.
53. Mollaamin, F.; Monajjemi, M. Fractal dimension on carbon nanotube-polymer composite materials using percolation theory. *J. Comput. Theor. Nanosci.* **2012**, *9*, 597-601, https://doi.org/10.1166/jctn.2012.2067.
54. Mollaamin, F.; Monajjemi, M. DFT outlook of solvent effect on function of nano bioorganic drugs. *Phys. Chem. Liq.* **2012**, *50*, 596-604, https://doi.org/10.1080/00319104.2011.646444.
55. Mollaamin, F.; Monajjemi, M. Doping of Graphene Nanostructure with Iron, Nickel and Zinc as Selective Detector for the Toxic Gas Removal: A Density Functional Theory Study. *C–Journal of Carbon Research.* **2023**, *9*, https://doi.org/10.3390/c9010020.
56. Monajjemi, M.; Khaleghian, M.; Tadayonpour, N.; Mollaamin, F. THE EFFECT OF DIFFERENT SOLVENTS AND TEMPERATURES ON STABILITY OF SINGLE-WALLED CARBON NANOTUBE: A QM/MD STUDY. Int. J. Nanosci. **2010**, *09*, 517-529, https://doi.org/10.1142/S0219581X10007071.
57. Mollaamin, F.; Monajjemi, M. Adsorption ability of Ga_5N_{10} nanomaterial for removing metal ions contamination from drinking water by DFT. *Int. J. Quantum Chem.* **2024**, *124*, e27348, https://doi.org/10.1002/qua.27348.
58. Mollaamin, F.; Monajjemi, M. Molecular modelling framework of metal-organic clusters for conserving surfaces: Langmuir sorption through the TD-DFT/ONIOM approach. *Mol. Simul.* **2023**, *49*, 365-376, https://doi.org/10.1080/08927022.2022.2159996.
59. Frisch, M. J.; Trucks, G. W.; Schlegel, H. B.; Scuseria, G. E.; Robb, M. A.; Cheeseman, J. R.; Scalmani, G.; Barone, V.; Petersson, G. A.; Nakatsuji, H.; Li, X.; Caricato, M.; Marenich, A. V.; Bloino, J.; Janesko, B. G.; Gomperts, R.; Mennucci, B.; Hratchian, H. P.; Ortiz, J. V.; Izmaylov, A. F.; Sonnenberg, J. L.; Williams-Young, D.; Ding, F.; Lipparini, F.; Egidi, F.; Goings, J.; Peng, B.; Petrone, A.; Henderson, T.; Ranasinghe, D.; Zakrzewski, V. G.; Gao, J.; Rega, N.; Zheng, G.; Liang, W.; Hada, M.; Ehara, M.; Toyota, K.; Fukuda, R.; Hasegawa, J.; Ishida, M.; Nakajima, T.; Honda, Y.; Kitao, O.; Nakai, H.; Vreven, T.; Throssell, K.; Montgomery, J. A., Jr.; Peralta, J. E.; Ogliaro, F.; Bearpark, M. J.; Heyd, J. J.; Brothers, E. N.; Kudin, K. N.; Staroverov, V. N.; Keith, T. A.; Kobayashi, R.; Normand, J.; Raghavachari, K.; Rendell, A. P.; Burant, J. C.; Iyengar, S. S.; Tomasi, J.; Cossi, M.; Millam, J. M.; Klene, M.; Adamo, C.; Cammi, R.; Ochterski, J. W.; Martin, R. L.; Morokuma, K.; Farkas, O.; Foresman, J. B.; Fox, D. J. Gaussian 16, Revision C.01, Gaussian, Inc., Wallingford CT, **2016.**
60. Dennington, R.; Keith, T.A.; Millam, J.M.J.S.I.S.M., KS, USA. GaussView 6.0. 16. **2016**, 143-150.
61. Mollaamin, F.; Monajjemi, M. Determination of GaN nanosensor for scavenging of toxic heavy metal ions (Mn^{2+}, Zn^{2+}, Ag^{+}, Au^{3+}, Al^{3+}, Sn^{2+}) from water: Application of green sustainable materials by molecular modeling approach. *Comput. Theor. Chem.* **2024**, *1237*, 114646, https://doi.org/10.1016/j.comptc.2024.114646.
62. Sciotto, R.; Ruiz Alvarado, I.A.; Schmidt, W.G. Substrate Doping and Defect Influence on P-Rich InP(001):H Surface Properties. *Surfaces* **2024**, *7*, 79-87, https://doi.org/10.3390/surfaces7010006.
63. Luo, J.; Wang, C.; Wang, Z.; Guo, Q.; Yang, J.; Zhou, R.; Matano, K.; Oguchi, T.; Ren, Z.; Cao, G.; Zheng, G.-Q. NMR and NQR studies on transition-metal arsenide superconductors $LaRu_2As_2$, $KCa_2Fe_4As_4F_2$, and $A_2Cr_3As_3$*. *Chinese Phys. B* **2020**, *29*, 067402, https://doi.org/10.1088/1674-1056/ab892d.
64. Mollaamin, F.; Monajjemi, M. Trapping of toxic heavy metals from water by GN–nanocage: Application of nanomaterials for contaminant removal technique. *J. Mol. Struct.* **2024**, *1300*, 137214, https://doi.org/10.1016/j.molstruc.2023.137214.

65. Morozov, E.V.; Il'ichev, A.V.; Bouznik, V.M. Magnetic Resonance Imaging Study of Water Absorption of Polymer Composite Materials Subjected to Mechanical and Temperature Impact. *Russ. J. Phys. Chem. B.* **2023**, *17*, 1361-1369, https://doi.org/10.1134/S1990793123060064.
66. Mollaamin, F.; Monajjemi, M. Application of DFT/TD-DFT Frameworks in the Drug Delivery Mechanism: Investigation of Chelated Bisphosphonate with Transition Metal Cations in Bone Treatment. *Chemistry* **2023**, *5*, 365-380. https://doi.org/10.3390/chemistry5010027.
67. Monajjemi, M.; Noei, M.; Mollaamin, F. Design of fMet-tRNA and Calculation of its Bonding Properties by Quantum Mechanics. *Nucleos. Nucleot. Acids* **2010**, *29*, 676-683, https://doi.org/10.1080/15257771003781642.
68. Mollaamin, F.; Shahriari, S.; Monajjemi, M. Influence of Transition Metals for Emergence of Energy Storage in Fuel Cells through Hydrogen Adsorption on the MgAl Surface. *Russ. J. Phys. Chem. B.* **2024**, *18*, 398-418, https://doi.org/10.1134/S199079312402026X.
69. Mollaamin, F. Computational Methods in the Drug Delivery of Carbon Nanocarriers onto Several Compounds in Sarraceniaceae Medicinal Plant as Monkeypox Therapy. *Computation* **2023**, *11*, 84. https://doi.org/10.3390/computation11040084.
70. Mollaamin, F.; Monajjemi, M. Transition metal (X = Mn, Fe, Co, Ni, Cu, Zn)-doped graphene as gas sensor for CO_2 and NO_2 detection: a molecular modeling framework by DFT perspective. *J. Mol. Model.* **2023**, *29*, 119, https://doi.org/10.1007/s00894-023-05526-3.
71. Mollaamin, F.; Monajjemi, M. The influence of Sc, V, Cr, Co, Cu, Zn as ferromagnetic semiconductors implanted on B_5N_{10}-nanocarrier for enhancing of NO sensing: An environmental eco-friendly investigation. *Comput. Theor. Chem.* **2024**, *1237*, 114666, https://doi.org/10.1016/j.comptc.2024.114666.
72. Agroskin, V.Y.; Bravy, B.G.; Vasiliev, G.K.; Guriev, V.I.; Kashtanov, S.A.; Chernyshev, Y.A. Investigation of the Interaction of Hydrogen Fluoride with Quartz by Measuring Surface Conductivity. *Russ. J. Phys. Chem. B.* **2023**, *17*, 1265-1269, https://doi.org/10.1134/S1990793123060131.
73. Trakhtenberg, L.I. Sensor Layers Based on Semiconductor Nanoparticles and Their Electronic Structure. *Russ. J. Phys. Chem. B.* **2023**, *17*, 600-607, https://doi.org/10.1134/S1990793123030144.
74. Aleksandrova, V.A.; Futoryanskaya, A.M. Influence of the Polymer Matrix Composition on the Size Range of Silver Nanoparticles Formed in a Succinyl Chitosan Solution Under the Action of Microwave Radiation. *Russ. J. Phys. Chem. B.* **2023**, *17*, 1394-1397, https://doi.org/10.1134/S1990793123060143.
75. Nemova, E.F.; Kobzeva, T.V.; Dultseva, G.G. Effect of the Radiation within Terahertz Range on the Transport Properties of Albumin: Binding with Metal Ions. *Russ. J. Phys. Chem. B.* **2024**, *18*, 95-100, https://doi.org/10.1134/S1990793124010354.
76. Shahriari, S.; Mollaamin, F.; Monajjemi, M. Increasing the Performance of {[(1-x-y) $LiCo_{0.3}Cu_{0.7}$] (Al and Mg doped)] O_2}, xLi_2MnO_3, $yLiCoO_2$ Composites as Cathode Material in Lithium-Ion Battery: Synthesis and Characterization. *Micromachines* **2023**, *14*, 241, https://doi.org/10.3390/mi14020241.
77. Mollaamin, F.; Monajjemi, M. Boron nitride doped with transition metals for carbon monoxide detection: a promising nanosensor for air cleaning. *Sensor Rev.* **2024**, *44*, 179-193, https://doi.org/10.1108/SR-01-2024-0066.

Publisher's Note & Disclaimer